coatings

Article

A Method of Improving the Structural Color Quality of HfO_2 Grating Based on Thin Film Filter

Chi Song [1,†], Xin Zhang [2,†], Mingyang Li [3], Zhenhao Liu [3], Henan Hu [3] and Zizheng Li [4,*]

1 School of Mechatronic Engineering and Automation, Foshan University, Foshan 528225, China
2 Jihua Laboratory, Foshan 528200, China
3 University of Chinese Academy of Sciences, Beijing 100039, China
4 School of Physics and Astronomy, Sun Yat-Sen University, Guangzhou 510275, China
* Correspondence: lizizh@mail.sysu.edu.cn
† These authors contributed equally to this work.

Abstract: In order to eliminate the influence of the high-order magnetic dipole modes in the short-wave range of the high-refractive-index dielectric grating, we propose a thin film filter to cut off the "useless" short-wave. In this way, the high-order magnetic dipole can be suppressed, and the quality of the structure color is highly improved after the thin film filter cut off the incident light in the non-resonant band. The combined application of the thin film filter and the grating filter not only avoids the problem of too big film layer thickness, but also reduces the manufacturing process cost. For example, the film system (basic film system 0.5 L H 0.5 L) and thickness of green, 15° and 45° incident film filters are 21 layers, 1.76 μm and 41 layers, 4.02 μm. The color coordinates corresponding to the calculation results occupy a large area on the Commission Internationale de l'Eclairage 1931 (CIE 1931) chromaticity diagram, which proves that this design scheme can effectively improve the structural color quality. This method obtains excellent theoretical simulation results. This has important implications for high-end imaging equipment and sensors.

Keywords: HfO_2 grating; thin film filter; structure color

check for updates

Citation: Song, C.; Zhang, X.; Li, M.; Liu, Z.; Hu, H.; Li, Z. A Method of Improving the Structural Color Quality of HfO_2 Grating Based on Thin Film Filter. *Coatings* **2022**, *12*, 1657. https://doi.org/10.3390/coatings12111657

Academic Editors: Martin Weis and Jaroslav Kovac

Received: 29 September 2022
Accepted: 25 October 2022
Published: 31 October 2022

1. Introduction

As the carrier of visual information in nature, color affects all aspects of human clothing, food, housing, and transportation [1–3]. With the rapid development of science and technology, human have higher and higher requirements for color quality. Traditional color dyes are not suitable for harsh environments and sophisticated systems [4]. Thin-film color filters are widely used in various precision optical systems. Ultra-narrow bandpass filters can produce high-quality colors, but the total thickness of the film layer often reaches tens of microns, and the requirements of the preparation process and equipment are extremely strict, which greatly increases the difficulty of preparation. Fabry–Perot (FP) cavity film (Metal-Insulator-Metal) realizes color filtration by adjusting the thickness of the intermediate medium layer (the thickness of the cavity), which has the advantages of low cost, simple design and manufacture [5–8], etc. Therefore, it is widely used. Considering that the extinction coefficient of metal materials cannot be ignored, the incident light is inevitably absorbed, thereby reducing the saturation and brightness of the color.

Driven by preparation methods such as nanoimprinting [9], photolithography/cite [10], and beam etching [11], we can see the shadow of metasurfaces in the fields of biomedicine [12], aerospace [13], energy [14], and communications [15,16]. Compared with thin-film color filters, the color quality of metasurface color filters has been greatly improved, but it is accompanied by problems such as higher cost. The physical mechanism of structural color generation is the modulation of optical properties such as phase, polarization, and amplitude of electromagnetic waves by metasurfaces. Based on the difference of materials, it can be divided into: plasmonic metasurface color filter [17–20] and all-dielectric metasurface color filter [21–24]. The local thermal damage caused by the absorption of metal materials greatly limits the application of plasma color filters. High-refractive-index all-dielectric filters have the advantages of low loss and high radiation efficiency and are one of the hotspots in current research. High-refractive-index dielectric (Si, Si_3N_4, TiO_2, etc.) metasurface structures based on Mie resonances, such as nano-blocks [25–27], disks [24,28], and gratings [29,30], have been demonstrated to yield high-purity structural colors. However, due to the influence of higher-order Mie resonances, it is difficult to obtain highly saturated structural colors with this metasurface color filter. This effect is most pronounced when getting red. In order to further improve the quality of structural color, researchers have proposed various schemes to suppress the generation of higher-order Mie resonances, such as adding antireflection coatings above and below the metasurface of high-refractive-index dielectrics [31]. This method increases the cost and difficulty of preparation while improving the color saturation. Si_3N_4 nano block designed by Jhen Hong Yang et al. uses Rayleigh scattering (RA) to suppress high-order Mie resonance in a short wavelength range by adjusting the structure size [32]. In order to consider high-saturation structural colors and reduce the cost and difficulty of fabrication, we carried out and published related research on the suppression of high-order dipole modes in the short-wave range of HfO_2 gratings. Based on Mie resonance mechanism of high refractive index dielectric materials, we obtained low full width of half maximum transmission (FWHM) (~2 nm) and high-quality factor Q (~424.5 nm) excellent characteristics after changing the duty cycle. It is of great significance for the application of sensors [30]. To find a low-cost and efficient means of inhibition will further expand its application areas.

In this paper, we have designed several all-dielectric filters for different structural colors in order to cut off the medium and short wavelengths of the incident light. In this way, after passing through the HfO_2 grating, there will be no higher-order dipole modes in the reflection spectrum of the "processed" band, which prevents the occurrence of this problem from the root. Filter and grating structures have high sensitivity to the angle of incidence, which also destroys the quality of the color spectrum. The structural color is enhanced at both 15° and 45° incident angles. Red and green are distributed around the contour of the chromaticity diagram. Comparing the positions of chromaticity coordinates on the CIE 1931 chromaticity diagram, it is proven that the proposed scheme can effectively improve the quality of structural color. This promotes the development of applications such as high-precision display imaging equipment.

2. Model Building and Simulation

The single-layer hafnium dioxide ($HfO_2 \approx 2.15$) grating constructed on K9 glass was simulated by the finite difference time domain method, and the reflection spectra under different grating sizes were obtained. The incident light was vertically incident on the grating, the X and Y directions of the simulation interval were set as periodic boundary conditions, and the Z direction was set as the PML boundary condition. A high precision mesh (mesh = 6) was selected. Figure 1a is a schematic diagram of the structure of the HfO_2 grating. The size, thickness, and period of the grating are defined as D, H, and T, respectively. The thickness H of the HfO_2 grating was 140 nm, fixed duty ratio (D/T = 4/7). During the change of the grating period from 240 nm to 420 nm, the resonance position of the reflection spectrum was flexibly regulated, as shown in Figure 1b. As the grating period increased, the intensity of the formant decreased gradually. Weaker higher-order dipole modes could be observed in the short-wave range, destroying the saturation of the structural colors. In order to prove the physical mechanism of the structural color generation, we analyzed the magnetic field distribution at the resonant peak position of the reflection spectrum when the grating period T = 385 nm (D = 220 nm), as shown in Figure 1c. The annular displacement current generated by the incident electromagnetic wave excited the magnetic dipole resonance, so that the magnetic field was confined in the high-refractive-index dielectric material HfO_2 grating.

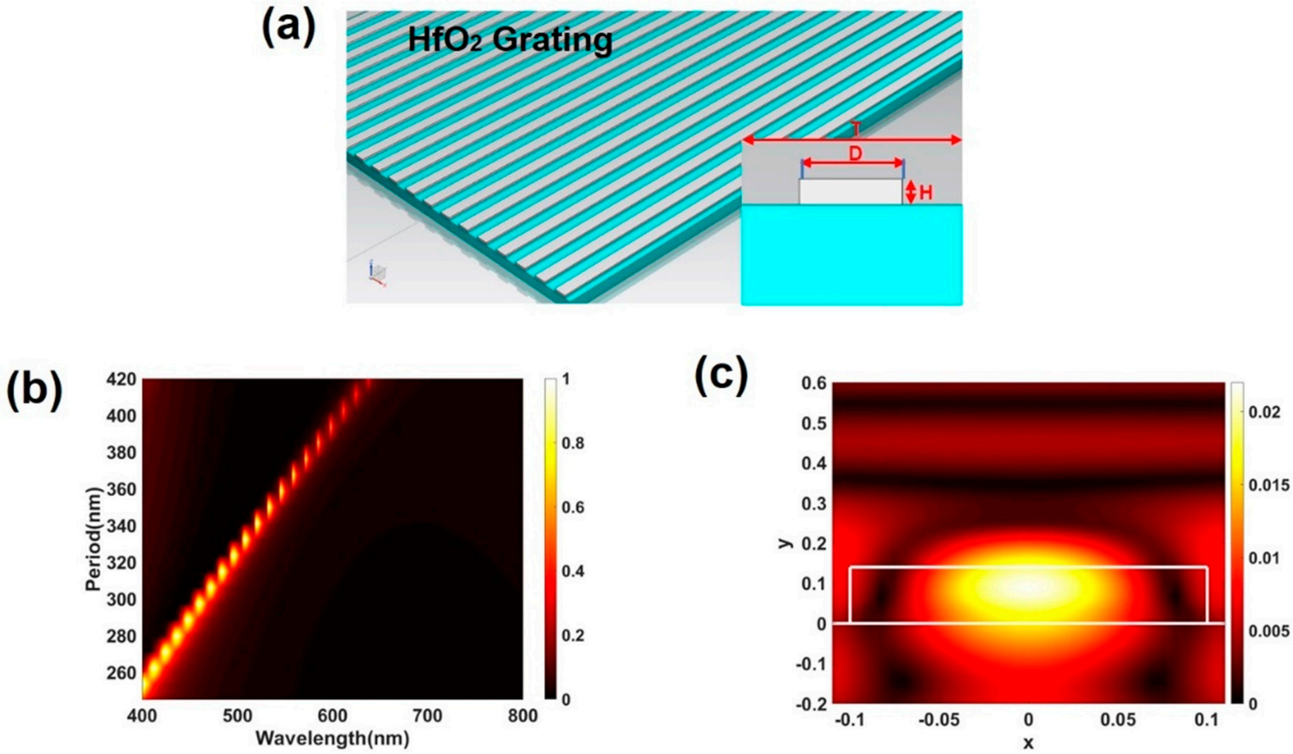

Figure 1. (**a**) Schematic diagram of the HfO_2 grating structure; (**b**) with a fixed duty ratio (D/T = 4/7) and grating thickness (H = 140 nm), the grating period T (from 240 nm to 420 nm) was swept; (**c**) the magnetic field distribution at the grating period T = 385 nm and the resonance peak λ = 533 nm.

After the incident light was filtered by the filter, the non-resonant region in the reflection spectrum was filtered, and the processed incident light was incident into the grating structure at the same incident angle θ (relative to the filter and grating), thereby improving the quality of the structure color, as Figure 2 shows. In order to cut off the short-wave region of the reflection spectrum, we used the thin film design software Essential Macleod to design filters with three different film systems. The initial film systems of the filters were respectively $(0.5\ L/H/0.5\ L)^n$. The coefficient n is an adjustment factor for the filter steepness, and the larger the coefficient, the higher the filter steepness. The high and low refractive index materials were tantalum pentoxide ($Ta_2O_5 \approx 2.14$) and silicon dioxide ($SiO_2 \approx 1.46$), respectively.

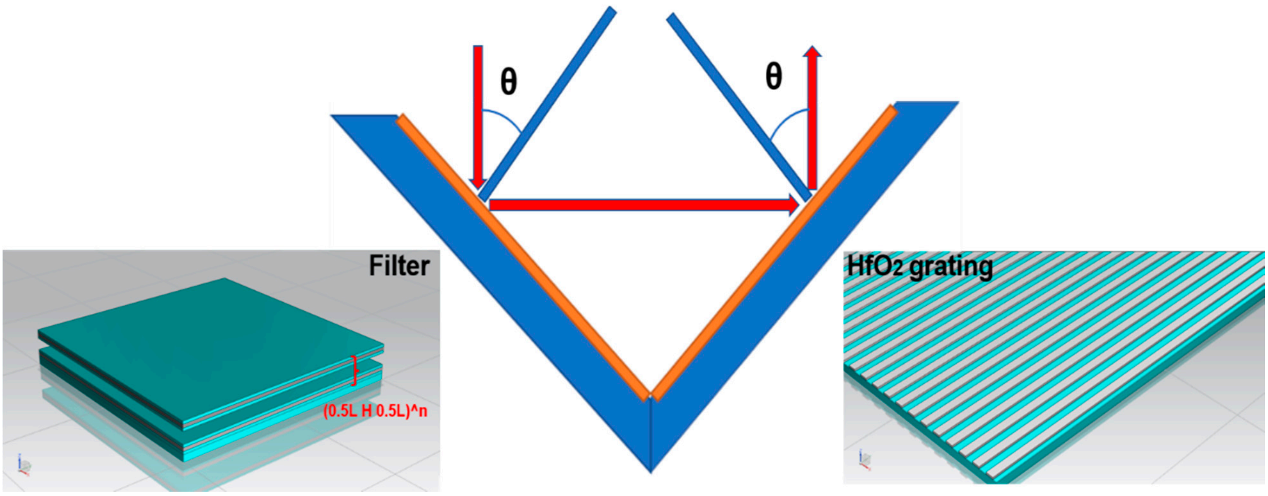

Figure 2. Schematic diagram of incident light after passing through filter and grating.

3. Results and Discussion

The equivalent interface method can be used to calculate the total reflectivity and transmissivity of multilayer dielectric films and metal films. The corresponding admittance results were obtained through the film characteristic matrix:

$$\begin{bmatrix} B \\ C \end{bmatrix} = \left\{ \prod_{j=1}^{K} \begin{bmatrix} \cos\delta_j & \frac{i}{\eta_j}\sin\delta_j \\ i\eta_j \sin\delta_j & \cos\delta_j \end{bmatrix} \right\} \begin{bmatrix} 1 \\ \eta_{K+1} \end{bmatrix} \tag{1}$$

where K is the total number of film layers, j is the jth layer of film, the multilayer film is equivalent to a single layer of film, the equivalent interface admittance $Y = C/B$, and the total reflectivity R is expressed as:

$$R = \left(\frac{\eta_0 B - C}{\eta_0 B + C}\right)\left(\frac{\eta_0 B - C}{\eta_0 B + C}\right)^* \tag{2}$$

Red, green, and blue are the three primary optical colors, which can be mixed in different proportions to present various colors. The RGB color purity determines the size of the triangle area of these three points on the chromaticity diagram. The area of the triangle in turn determines the number of colors that can be combined. Figure 3a–c are the spectral responses of the incident light incident on the filter and HfO_2 grating at an incident angle of 15°, corresponding to blue, green, and red in the optical three primary colors, respectively. The cut-off wavelengths of the filters were 436 nm, 518 nm, and 589 nm, respectively. The number of film layers for red, green, and blue filters were 51, 21, and 21, respectively. The total film thickness of each film layer was 5.052 µm, 1.76 µm, and 1.426 µm, respectively. The reflectivity of the filter is defined as R_1, and the reflectivity of the HfO_2 grating is defined as R_2. Without considering other optical losses, the final reflectivity of the entire system is $R_{final} = R_1 \times R_2$. The passband part had high transmittance, and the transmittance exceeded 99%. This means that the function of the filter in the whole system was only the short-wave range cut-off, and the impact on the real working band was minimal. Figure 3d–f are the final response of the reflectance spectrum after filtering and HfO_2 grating. The results show that the filter had almost no effect on the spectrum in the long-wave range after filtering the short-wave.

As the angle of incidence increased, the reflectance spectra of the filter and grating structures were severely damaged, affecting the quality of the colors produced. The high sensitivity to angle makes them unsuitable for working conditions of large angle incidence. We further explored the color quality at an incident angle of 45°. In order to reduce the cost of the filter, only the short-wave reflection cut-off and the transmission cut-off near the resonance wavelength were constrained in the design process. Figure 4a–c are the spectral responses of the filter and the HfO_2 grating at an incident angle of 45°, corresponding to blue, green, and red in the optical three primary colors, respectively. The cut-off wavelengths of the filters were 439 nm, 472 nm, and 567 nm, respectively. The number of film layers for red, green, blue filter films was 41, 41, and 31 respectively. The total film thickness of each film layer was 4.594 µm, 4.02 µm, and 2.44 µm. The black curve corresponds to the reflectance spectrum of the filter, and the red curve corresponds to the reflectance spectrum of the HfO_2 grating structure. With the increase of the incident angle, the peak intensity was greatly reduced and the side-peak interference at the off-resonant peak position became more obvious. Figure 4d–f are the final responses of the reflectance spectrum after filtering and HfO_2 grating. Although the short wave was effectively cut off, the increase of the angle will cause the side peak interference at the non-resonant position to be obvious.

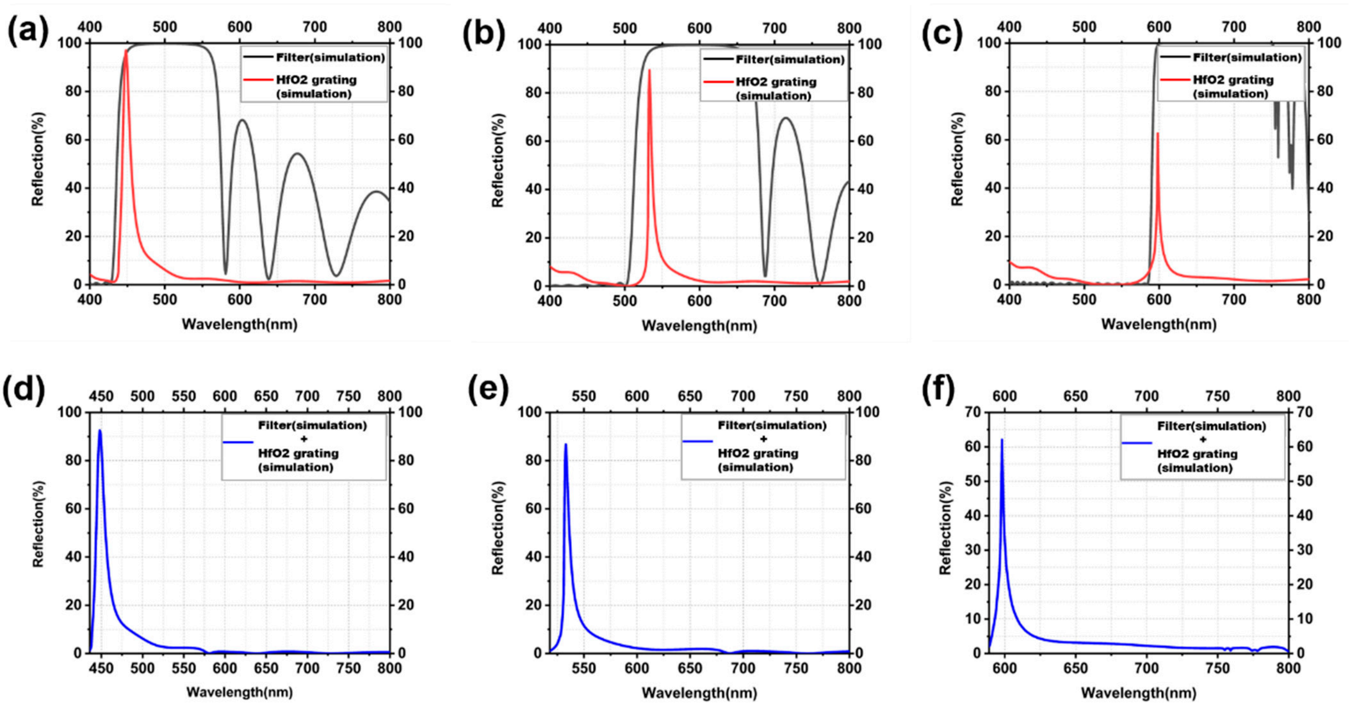

Figure 3. The light was incident at 15°, (**a**–**c**) correspond to the blue, green, red, black lines in the optical three primary colors represent the reflection spectrum of the filter, and the red line represents the reflection spectrum of the HfO_2 grating. (**d**–**f**) Reflectance spectra of filters and HfO_2 gratings.

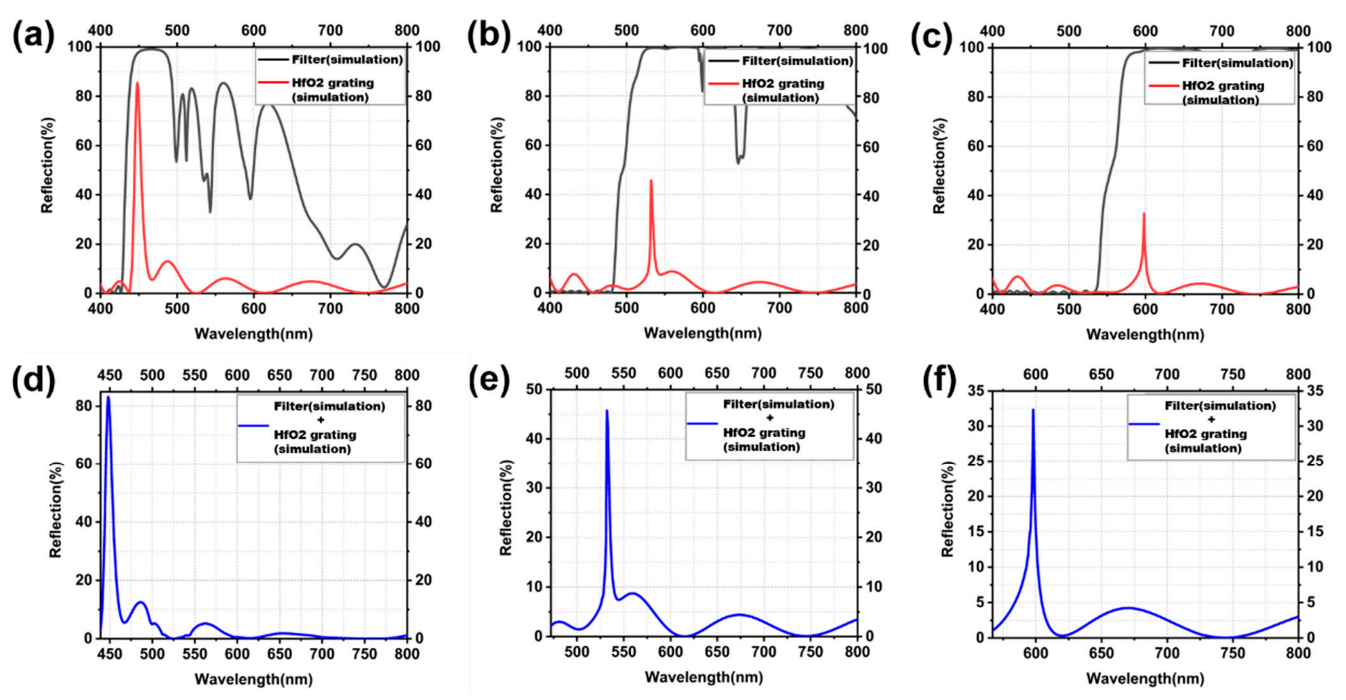

Figure 4. The light is incident at 45°, (**a**–**c**) correspond to the blue, green, red, and black lines in the optical three primary colors represent the reflection spectrum of the filter, and the red line represents the reflection spectrum of the HfO_2 grating. (**d**–**f**) Reflectance spectrum of filter and HfO_2 grating.

The location of the chromaticity coordinates on the chromaticity diagram is undoubtedly one of the best ways to judge the quality of structural colors. The CIE 1931 chromaticity diagram describes a color space mathematically. Chromaticity coordinates are defined as

(x, y), which are calculated from tristimulus values (X, Y, Z), $x = X/(X + Y + Z)$, $y = Y/(X + Y + Z)$. Tristimulus values are determined by Equations (3)–(5) [31]:

$$X = \frac{1}{k}\int D(\lambda)\overline{x}(\lambda)R(\lambda)d\lambda \quad (3)$$

$$Y = \frac{1}{k}\int D(\lambda)\overline{y}(\lambda)R(\lambda)d\lambda \quad (4)$$

$$Z = \frac{1}{k}\int D(\lambda)\overline{z}(\lambda)R(\lambda)d\lambda \quad (5)$$

where $R(\lambda)$ represents the reflection spectrum, $D(\lambda)$ represents the energy distribution of the illumination, and $\overline{x}$, $\overline{y}$ and $\overline{z}$ represent the color vision parameters of the standard observer human eye. The chromaticity coordinates were calculated by the above formula, and the chromaticity coordinates of HfO_2 grating and "HfO_2 grating + filter" were drawn on the CIE 1931 chromaticity diagram under the incident angles of 15° and 45° to form an intuitive comparison, as shown in Figure 5. "o" and "*" are the chromaticity coordinates of HfO_2 grating and "HfO_2 grating + filter" under 15° incident angle, respectively; "x" and "+" are the chromaticity coordinates of HfO_2 grating and "HfO_2 grating + filter" under 45° incident angle, respectively. The distribution range of RGB three colors obtained at 15° incidence angle in the chromaticity map was far beyond the simulation results reported by Jhen Hong Yang et al. [32], which means that this method effectively improves the color quality. With the increase of the angle, the chromaticity coordinates of the three colors of RGB moved to the center of the chromaticity diagram, the area enclosed by the three became smaller and smaller, and the structural color quality of the HfO_2 grating is obviously reduced. The use of filters effectively overcame this problem, and the chromaticity coordinates of the three primary colors corresponding to the incident angles of 15° and 45° approached the contour position of the chromaticity diagram. The color quality of the 15° and 45° incident angles incident on the "filter + grating" was significantly improved compared to the HfO_2 grating alone, but the color quality of any combination will decrease with the increase of the incident angle.

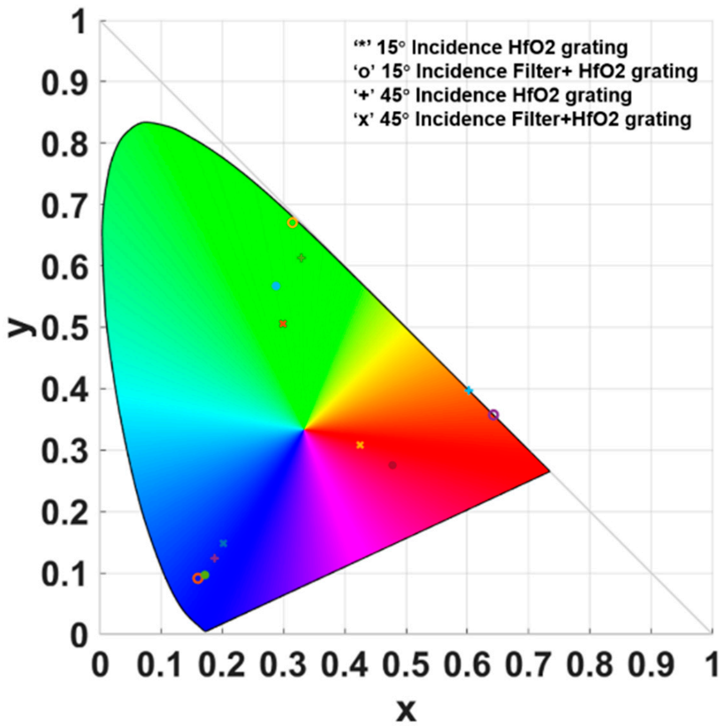

Figure 5. The distribution of chromaticity coordinates of the HfO_2 grating and the "filter + HfO_2 grating" on the CIE 1931 chromaticity diagram at the incident angles of 15° and 45°.

The structural colors obtained by several combinations were compared, as shown in Figure 6. Figure 6a,b are the blue, green, and red obtained by the HfO_2 grating and the "Filter + HfO_2 grating" at 15° and 45° incident angles, respectively. The highest quality of structural color was obtained with the "Filter + HfO_2 grating" at an incident angle of 15°. The red and green qualities obtained by the four combinations were from high to low: "15° + Filter + HfO_2 grating" > "45° + Filter + HfO_2 grating" > "15° + HfO_2 grating" > "45° + HfO_2 grating". The blue produced by both combinations at 45° incidence were of lower quality than the blue obtained at 15°.

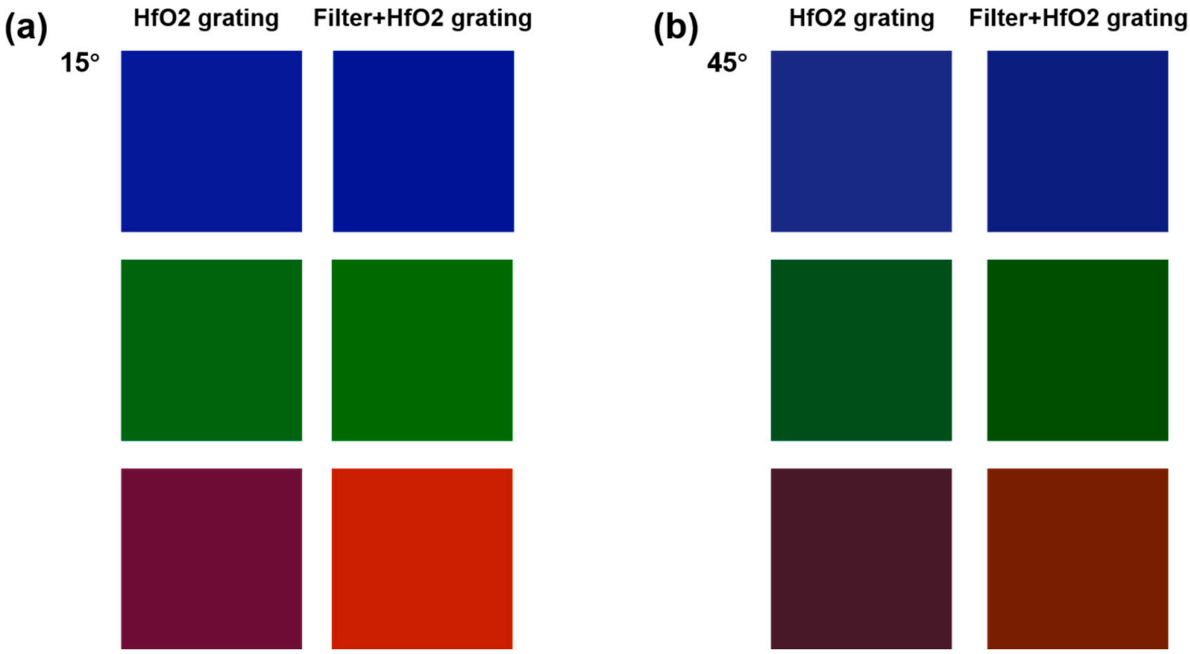

Figure 6. (**a**,**b**) are the blue, green and red obtained by incident on the HfO_2 grating and the "filter + HfO_2 grating" at 15° and 45° incident angles, respectively.

4. Conclusions

In conclusion, in order to suppress the high-order dipole modes generated by the high-refractive-index dielectric material HfO_2 grating in the short-wave direction, we propose to use a filter to directly filter the short-wave non-resonant region, thereby retaining the true working band. The simulation results verify the feasibility of this method. Considering the high sensitivity of the HfO_2 grating to the angle of incidence, this also destroys the color quality. In order to illustrate the impact of the incident angle on the color quality, we discussed the structure colors obtained at the incident angle of 15° and 45° and compared the extent to which this method can improve the color quality. The chromaticity coordinate distributions at incident angles of 15° and 45° were calculated and compared, and it was proven that this method can effectively improve the saturation of structural colors and obtain high-quality colors at large angles. The color quality can be improved by using thin film filters to suppress higher-order dipole modes. Compared with the method of multilayer all dielectric nanostructures to suppress higher-order dipole modes, this method reduces the difficulty and cost in preparation. This research provides a new idea for suppressing higher-order dipole modes, which can be applied in imaging devices with demanding precision and metrics, and sensors for the visible light range.

Author Contributions: Conceptualization, C.S. and Z.L. (Zizheng Li); methodology, X.Z.; software, M.L.; validation, C.S., X.Z., and Z.L. (Zizheng Li); formal analysis, Z.L. (Zhenhao Liu); investigation, H.H.; resources, H.H.; data curation, C.S.; writing—original draft preparation, C.S.; writing—review and editing, Z.L. (Zizheng Li); visualization, X.Z.; supervision, X.Z.; project administration, X.Z.; funding acquisition, C.S. All authors have read and agreed to the published version of the manuscript.

Funding: This research was funded by the Guangdong Basic and Applied Basic Research Foundation (2020A1515110259).

Institutional Review Board Statement: Not applicable.

Informed Consent Statement: Not applicable.

Data Availability Statement: The data presented in this study are available on request from the corresponding author.

Conflicts of Interest: The authors declare no conflict of interest.

References

1. Spence, C. The Psychological Effects of Food Colors. In *Handbook on Natural Pigments in Food and Beverages*; Woodhead Publishing: Shaston, UK, 2016; pp. 29–58.
2. Crowley, A.E. The two-dimensional impact of color on shopping. *Mark. Lett.* **1993**, *4*, 59–69. [CrossRef]
3. Gurses, A.; Acikyildiz, M.; Guneş, K.; Gurses, M.S. *Dyes and Pigments: Their Structure and Properties*; SpringerBriefs in Green Chemistry for Sustainability; Springer: Cham, Switzerland; Berlin/Heidelberg, Germany, 2016; pp. 13–29.
4. Landy, N.I.; Sajuyigbe, S.; Mock, J.J.; Smith, D.R.; Padilla, W.J. Perfect metamaterial absorber. *Phys. Rev. Lett.* **2008**, *100*, 207402. [CrossRef] [PubMed]
5. He, Y.; Deng, H.; Jiao, X.; He, S.; Gao, J.; Yang, X. Infrared perfect absorber based on nanowire metamaterial cavities. *Opt. Lett.* **2013**, *38*, 1179–1181. [CrossRef] [PubMed]
6. Liu, Z.; Liu, X.; Huang, S.; Pan, P.; Chen, J.; Liu, G.; Gu, G. Automatically Acquired Broadband Plasmonic-Metamaterial Black Absorber during the Metallic Film-Formation. *ACS Appl. Mater. Interfaces* **2015**, *7*, 4962–4968. [CrossRef] [PubMed]
7. Durmaz, H.; Cetin, A.E.; Li, Y.; Paiella, R. A Polarization Insensitive Wide-Band Perfect Absorber. *Adv. Eng. Mater.* **2019**, *21*, 1900188. [CrossRef]
8. Wang, W.; Qu, Y.; Du, K.; Bai, S.; Tian, J.; Pan, M.; Ye, H.; Qiu, M.; Li, Q. Broadband optical absorption based on single-sized metal-dielectric-metal plasmonic nanostructures with high-ε00 metals. *Appl. Phys. Lett.* **2017**, *110*, 101101. [CrossRef]
9. Ge, J.; Ding, B.; Hou, S.; Manlin, L.; Donguk, N.; Hongwei, D.; Huajian, G.; Yee Cheong, L.; Hong, L. Rapid fabrication of complex nanostructures using room-temperature ultrasonic nanoimprinting. *Nat. Commun.* **2021**, *12*, 3146. [CrossRef]
10. Badloe, T.; Kim, J.; Kim, I. Liquid crystal-powered Mie resonators for electrically tunable photorealistic color gradients and dark blacks. *Light Sci. Appl.* **2022**, *11*, 118. [CrossRef]
11. Kim, T.; Yu, E.S.; Bae, Y.G. Asymmetric optical camouflage: Tuneable reflective colour accompanied by the optical Janus effect. *Light Sci. Appl.* **2020**, *9*, 175. [CrossRef]
12. Deniz, U.Y.; Amir, G.; Mahmut, C.S.; Murat, G.; Ahmet, T.; Bayram, B.; Ekmel, O. Colorimetric and Near-Absolute Polarization-Insensitive Refractive-Index Sensing in All-Dielectric Guided-Mode Resonance Based Metasurface. *J. Phys. Chem. C* **2019**, *123*, 19125–19134.
13. Joy, V.; Dileep, A.; Abhilash, P.V. Metasurfaces for Stealth Applications: A Comprehensive Review. *J. Electron. Mater.* **2021**, *50*, 3129–3148. [CrossRef]
14. Fei, C.; Sun, T.; Cao, F. Metallic nanostructures for light trapping in energy-harvesting devices. *Light Sci. Appl.* **2014**, *3*, 161.
15. Zhang, X.G.; Sun, Y.L.; Zhu, B. A metasurface-based light-to-microwave transmitter for hybrid wireless communications. *Light Sci. Appl.* **2022**, *11*, 126. [CrossRef]
16. Xu, L.; Rahmani, M. Programmable structured surfaces can change the future of wireless communications. *Light Sci. Appl.* **2022**, *11*, 196. [CrossRef]
17. Yoon, Y.T.; Park, C.H.; Lee, S.S. Highly efficient color filter incorporating a thin metal–dielectric resonant structure. *Appl. Phys. Express* **2012**, *5*, 022501. [CrossRef]
18. Mazulquim, D.B.; Lee, K.J.; Yoon, J.W.; Muniz, L.V.; Borges, B.H.V.; Neto, L.G.; Magnusson, R. Efficient band-pass color filters enabled by resonant modes and plasmons near the Rayleigh anomaly. *Opt. Express* **2014**, *22*, 30843–30851. [CrossRef]
19. Zeng, B.; Gao, Y.; Bartoli, F.J. Ultrathin Nanostructured Metals for Highly Transmissive Plasmonic Subtractive Color Filters. *Sci. Rep.* **2013**, *3*, 2840. [CrossRef]
20. Reibold, D.; Shao, F.; Erdmann, A.; Peschel, U. Extraordinary low transmission effects for ultra-thin patterned metal films. *Opt. Express* **2009**, *17*, 544–551. [CrossRef] [PubMed]
21. Overvig, A.C.; Shrestha, S.; Malek, S.C. Dielectric metasurfaces for complete and independent control of the optical amplitude and phase. *Light Sci. Appl.* **2019**, *8*, 92. [CrossRef]
22. Julien, P.; Frederic, B.; Bruno, G.; Igor, O.; Nicolas, B. All-Dielectric Colored Metasurfaces with Silicon Mie Resonators. *ACS Nano* **2016**, *10*, 7761–7767.
23. Flauraud, V.; Reyes, M.; Paniagua-Domínguez, R.; Kuznetsov, A.I.; Brugger, J. Silicon Nanostructures for Bright Field Full Color Prints. *ACS Photonics* **2017**, *4*, 1913–1919. [CrossRef]
24. Park, C.S.; Shrestha, V.R.; Yue, W.J.; Gao, S.; Lee, S.S.; Kim, E.S.; Choi, D.Y. Structural Color Filters Enabled by a Dielectric. Metasurface Incorporating Hydrogenated Amorphous Silicon Nanodisks. *Sci. Rep.* **2017**, *7*, 2556. [CrossRef]

25. Nagasaki, Y.; Suzuki, M.; Takahara, J. All-Dielectric Dual-Color Pixel with Subwavelength Resolution. *Nano Lett.* **2017**, *17*, 7500–7506. [CrossRef] [PubMed]
26. Sun, S.; Zhou, Z.; Zhang, C.; Gao, Y.; Duan, Z.; Xiao, S.; Song, Q. All -Dielectric Full-Color Printing with TiO_2 Metasurfaces. *ACS Nano* **2017**, *11*, 4445–4452. [CrossRef] [PubMed]
27. Bao, Y.; Yu, Y.; Xu, H.; Guo, C.; Li, J.; Sun, S.; Zhou, Z.K.; Qiu, C.W.; Wang, X.H. Full-colour nanoprint-hologram synchronous metasurface with arbitrary hue-saturation-brightness control. *Light Sci. Appl.* **2019**, *8*, 95. [CrossRef]
28. Park, C.S.; Koirala, I.; Gao, S.; Shrestha, V.R.; Lee, S.S.; Choi, D.Y. Structural color filters based on an all-dielectric metasurface exploiting silicon-rich silicon nitride nanodisks. *Opt. Express* **2019**, *27*, 667–679. [CrossRef]
29. Wu, Y.K.R.; Hollowell, A.E.; Zhang, C.; Guo, L.J. Angle-Insensitive Structural Colours based on Metallic Nanocavities and Coloured Pixels beyond the Diffraction Limit. *Sci. Rep.* **2013**, *3*, 1194. [CrossRef]
30. Zhao, Y.H.; Li, Z.Z.; Liu, X.Y.; Wang, K.; Sun, Y.Q.; Yang, H.G.; Wang, X.Y.; Wang, T.T.; Song, N.T.; Gao, J.S. Multi-layered all-dielectric grating visible color filter with a narrow band and high-quality factor. *Opt. Express* **2022**, *30*, 22820–22829. [CrossRef]
31. Yang, B.; Liu, W.W.; Li, Z.C.; Cheng, H.; Choi, D.Y.; Chen, S.Q.; Tian, J.G. Ultra-highly Saturated Structural Colors Enhanced by Multipolar-Modulated Metasurfaces. *Nano Lett.* **2019**, *19*, 4221–4228. [CrossRef]
32. Yang, J.H.; Babicheva, V.E.; Yu, M.W.; Lu, T.C.; Lin, T.R.; Chen, K.P. Structural Colors Enabled by Lattice Resonance on Silicon Nitride Metasurfaces. *ACS Nano* **2020**, *14*, 5678–5685. [CrossRef]